Universiteit Leiden
The Netherlands

Blood flow dynamics in the total cavopulmonary connection long-term after Fontan completion
Rijnberg, F.M.

CHAPTER 8

4D flow MRI derived energetics in the Fontan circulation correlate with exercise capacity and cT1 liver mapping

Friso M. Rijnberg, Jos J.M. Westenberg, Hans C. van Assen, Joe F. Juffermans, Lucia J.M. Kroft, Pieter J. van den Boogaard, Covadonga Terol Espinosa de Los Monteros, Evangeline G. Warmerdam, Tim Leiner, Heynric B. Grotenhuis, Monique R.M. Jongbloed, Mark G. Hazekamp, Arno A.W. Roest, Hildo J. Lamb

Abstract

Aim

This study explores the relationship between in vivo 4D flow MRI derived blood flow energetics in the TCPC, exercise capacity and MRI-derived liver fibrosis/congestion.

Background

The Fontan circulation, in which both caval veins are directly connected with the pulmonary arteries (i.e. the total cavopulmonary connection ,TCPC) is the palliative approach for single ventricle patients. Blood flow efficiency in the TCPC has been associated with exercise capacity and liver fibrosis using in silico computational fluid dynamic modelling. Nowadays, 4D flow MRI allows for assessment of in vivo blood flow energetics, including kinetic energy (KE) and viscous energy loss rate (EL).

Methods

Fontan patients were prospectively evaluated using a comprehensive cardiovascular and liver MRI protocol, including 4D flow imaging of the TCPC, between 2018-2021. Peak VO2 was determined using cardiopulmonary exercise testing (CPET). Iron-corrected whole liver T1 mapping was performed as a marker of liver fibrosis/congestion (cT1). KE and EL in the TCPC were computed from 4D flow MRI and normalized for inflow. Furthermore, blood flow energetics were compared between standardized segments of the TCPC.

Results

Sixty-two Fontan patients were included (53% male, mean age 17.3±5.1 years). Maximal effort CPET was obtained in 50 patients (mean peak VO2 27.1±6.2 ml/kg/min, 56±12% of predicted). Both KE and EL in the entire TCPC (n=28) were significantly correlated with cT1 (r=0.50, p=0.006 and r=0.39, p=0.04, respectively), peak V02 (r=-0.61, p=0.003 and r=-0.54, p=0.009, respectively) and predicted peak V02 (r=-0.44, p=0.04 and r=-0.46, p=0.03, respectively). Segmental analysis indicated that the most adverse flow energetics were found in the Fontan tunnel and left pulmonary artery.

Conclusions

Adverse 4D flow MRI derived kinetic energy and viscous energy loss rate in the TCPC correlate with decreased exercise capacity and increased levels of liver fibrosis/ congestion. 4D flow MRI is promising as a non-invasive screening tool for identification of patients with adverse TCPC flow efficiency that may guide treatment strategies during follow-up.

Introduction

The Fontan procedure provides a unique surgical solution for congenital heart disease patients with a functionally univentricular heart defect, by connecting the systemic venous return directly with the pulmonary arteries (i.e. the total cavopulmonary connection: TCPC). Consequently, the Fontan circulation requires increased central venous pressure (CVP) to overcome the serial resistance in the TCPC and pulmonary vascular bed to maintain an adequate cardiac output. The chronic exposure to elevated venous pressures provides a significant burden for upstream organs, including an almost universal occurrence of liver fibrosis.[1] Furthermore, the ability to increase preload and thereby cardiac output during exercise is limited leading to a diminished exercise capacity.[2]

Being one of the few modifiable factors in the Fontan circulation, blood flow efficiency in the TCPC has been widely studied using predominantly in silico computational fluid dynamic (CFD) models.[3-5] Highly variable blood flow efficiency in the TCPC has been reported, related to the presence of energy-consuming geometric factors that can become apparent during follow-up.[3, 5] Recently, correlations were found between CFD-derived TCPC blood flow efficiency and clinical outcome, including liver fibrosis[6] and exercise capacity.[7]

Drawbacks of CFD modelling are that it is time-consuming and requires expert knowledge and infrastructure, limiting widespread use in clinical care. 4D flow magnetic resonance imaging (MRI) is emerging as a non-invasive screening tool for visualization of energy-consuming flow patterns in the TCPC and quantification of flow-related hemodynamic parameters including kinetic energy (KE) and viscous energy loss rate (EL).[8-10] The hypothesis in this study is that these in vivo 4D flow MRI-derived energetics in the TCPC are associated with exercise capacity and liver fibrosis/congestion. Subsequently, the aim of this study is to determine KE and EL in the TCPC using 4D flow MRI and assess the relationship with exercise capacity and MR-based assessment of liver fibrosis/congestion.

Materials and methods

Study population

Sixty-two Fontan patients were prospectively evaluated using a comprehensive cardiovascular and liver MRI protocol, including 4D flow imaging of the TCPC, between

8

2018-2021 at the Leiden University Medical Center. All patients >8 years old without contraindications for MRI were eligible for inclusion.

Cardiopulmonary exercise testing

Cardiopulmonary exercise testing (CPET) was performed on an upright bicycle ergometer (GE Healthcare, Wisconsin, USA) including peak oxygen uptake assessment (VO2). CPET was performed on the same day or within 6 months of MRI. A continuous incremental bicycle protocol was executed according to the Godfrey protocol.[11] Peak VO2 (ml/kg/min) and percentage of predicted peak V02 (%) were determined in all patients that achieved maximal effort (respiratory exchange ratio >1.0) using previously reported reference values.[12]

Laboratory data

Standard laboratory assessment was performed on the same day or within 6 months of MRI, including liver enzymes, total protein, albumin, total bilirubin, and international normalized ratio (INR). Additionally, a feces sample was tested on alfa-1-antitrypsin excretion as a marker of (early) protein losing enteropathy. Results were interpreted using the hospital's standard age- and gender-specific reference values.

Magnetic resonance imaging

All MRI examinations were performed on a 3T Philips scanner (Ingenia, Philips Healthcare, Best, the Netherlands).

Multiparametric Liver imaging

Patients underwent multiparametric liver imaging using proton density fat-fraction (PDFF), T2*, and iron-corrected T1 mapping (cT1) for the assessment of liver fat, iron, and fibrosis/inflammation/congestion, respectively (Liver MultiScan™, Perspectum Diagnostics Ltd., Oxford, UK).[13] Patients underwent liver imaging after fasting for at least 4 hours. No intravenous contrast agent was used. Values were calculated from segmentation of whole liver regions (cT1 and PDFF) or one or more regions of interest (T2*) on one or more transversal slices. cT1 mapping allows for quantification of extracellular fluid in the liver, which is increased in both liver fibrosis, inflammation and venous congestion. Since inflammation is usually absent in liver fibrosis in Fontan patients[14] and liver enzymes are usually normal or only mildly elevated, elevated cT1 values in Fontan patients will predominantly reflect fibrosis and/or venous congestion. Reference values of PDFF, T2* and cT1 are <5.6%, >12.5ms and 633-794ms, respectively.[15-17] All liver scans were anonymized and subsequently analyzed by Perspectum Diagnostics (Oxford, UK) using an online portal.

Ventricular function

Ventricular ejection fraction and cardiac output were calculated by ventricular volume analysis (MASS software, Leiden, the Netherlands) of multislice two-dimensional cine transversal images using a steady-state-free-precession sequence. The cardiac index was derived by normalizing cardiac output for body surface area (Haycock).

4D flow MRI

Patients underwent retrospective ECG- and respiratory navigator-gated 4D flow MRI examination dedicated for imaging of the TCPC. Acquisition details for 4D flow MRI are covered in Supplemental Table 1.

A 3D reconstruction of the TCPC was semi-automatically segmented on magnitude-weighted speed images of a time-averaged reconstruction of the 4D flow velocity field (CAAS v5.1, MR Solutions, Pie Medical Imaging). The region of interest covered the area between the Fontan tunnel (above entry of the hepatic veins), SVC (below the brachiocephalic vein) and the right- and left pulmonary arteries (PAs) up to the levels of the segmental branches. The right upper lobe branch was excluded from the segmentation since the resolution of the 4D flow MRI for this small vessel is insufficient.

Both the KE and EL of blood flow in the TCPC were computed from the 4D flow MRI velocity field using in-house developed software, as previously described.[18] KE represents the amount of energy in the blood flow due to its motion. EL represents the rate of kinetic energy lost in the blood flow due to friction and can be computed from three-dimensional velocity gradients derived from 4D flow MRI. EL was computed using the viscous dissipation function from the Navier-Stokes equation, assuming laminar blood flow.[18] The total amount of KE (in milliJoule, [mJ]) and EL (in milliwatts, mW) within the TCPC is computed by summing voxel-wise energetics for each time-phase (24 phases per cardiac cycle). The cardiac-cycle averaged values are reported. In patients in whom the entire TCPC was available for analysis, energetics were normalized for inflow (SVC + Fontan tunnel flow, in L/min); KE_{norm_flow} in mJ per L/min and EL_{norm_flow} in mW per L/min.[19]

Segmental analysis

To further explore and compare the energetics in the specific components of the TCPC, a sub analysis was performed to determine segment-specific energetics (Fontan tunnel, central Fontan confluence, SVC, LPA and RPA), using in-house developed software as previously described.[19] Additional benefit of this approach is that in patients with a fenestration closure device or PA stent in situ, in whom the entire TCPC cannot be segmented because of device-related flow artefacts, energetics in the TCPC segments without device-related artefacts can still be studied. In these patients, only part of the Fontan tunnel (distal to the device) or PA (proximal to the stent) can be included in

the segmentation. Segments with a length <1.5cm were excluded from the analysis to ensure sufficient voxels for energetic analysis.[19]

In summary, the TCPC was automatically divided into 5 segments. Energetics within each segment were normalized for segment-specific inflow (Fontan confluence) or inflow + length (Fontan tunnel, SVC, LPA, RPA; $KE_{norm\_flow+length}$ and $EL_{norm\_flow+length}$).[19] Cross-sectional areas (CSA) normalized for BSA of the included conduit, SVC, LPA and RPA segments were determined perpendicularly to their centerlines at a 1mm interval.[20] The mean CSA of each segment is reported.

Statistical analysis

Continuous data were presented as mean (standard deviation) or median (interquartile range, IQR), as appropriate. Normal distributions of continuous data were tested using the Shapiro-Wilk test. Pearson and/or Spearman correlation analysis (weak 0.3-0.5, moderate 0.5-0.7, strong ≥0.7-0.9 and excellent >0.9) was performed between the main endpoints (cT1 liver mapping and maximal exercise capacity) and MRI parameters; ventricular function and 4D flow energetics in the entire TCPC. Segment-specific energetics (Fontan tunnel, SVC, LPA and RPA) were compared with each other using the Kruskal Wallis test (adjusted by the Bonferroni method for multiple tests). Correlation analysis was performed between segment-specific energetics and normalized CSA. A p-value <0.05 was considered statistically significant. Data were analyzed with SPSS 25.0 (IBM Corp., Armonk, NY, USA) and GraphPad Prism 8.0 (GraphPad Software, La Jolla, California, USA).

Results

Study population

Patient characteristics are shown in Table 1. Fifty-three percent of patients was male. Mean age at MRI of 17.3±5.1 years and mean time between Fontan completion and MRI was 13.6±4.8 years. The majority of patients (94%) underwent Fontan completion using a (fenestrated) 16-20mm extracardiac Goretex conduit. Fenestrations closed spontaneously or were routinely closed after Fontan completion using a fenestration closure device. One patient still had a patent fenestration at time of MRI. All but two patients were in good clinical condition (New York Heart Association class I-II).

Table 1. Patient characteristics

Male/Female, n	33/29
Primary diagnosis, n (%)	
- TA	14(23)
- HLHS	12(19)
- DILV + TGA	10(16)
- DORV	6(10)
- uAVSD	5(8)
- ccTGA	5(8)
- PA + IVS	5(8)
- Other	5(8)
Dominant ventricle	
Left, n (%)	35(56)
Right, n (%)	21(34)
Biventricular/indeterminate, n (%)	6(10)
Characteristics at Fontan procedure	
Previous bidrectional Glenn shunt, n(%)	62 (100)
Age at Fontan, years	3.7(1.8)
Fontan technique LT/ECC	4/58
Implanted conduit size (16/18/20mm), n	30/22/6
Fenestration, n(%)	38(61)
Characteristics at time of MRI	
Age at MRI, years	17.3(5.1)
Height, cm	167(12)
BSA, m^2	1.6(0.3)
Time between Fontan and MRI, years	13.6(4.8)
NYHA-class I-II, n (%)	60(97)

Values are reported as mean (standard deviation) unless otherwise specified. TA; tricuspid atresia, HLHS; hypoplastic left heart syndrome, DILV; double inlet left ventricle, (cc)TGA; (congenital corrected) transposition of the great arteries, DORV; double outlet right ventricle, uAVSD; unbalanced atrioventricular septal defect, PA+IVS; pulmonary atresia with intact ventricular septum, LT; lateral tunnel, ECC; extracardiac conduit

CPET and laboratory

CPET results are presented in Table 2. CPET was performed in 57 patients (92%), with 50 patients achieving maximal effort. Mean peak VO2 was 27.1±6.2 ml/kg/min, 57%±12% of predicted peak VO2.

Laboratory results are provided in Table 3. Total protein and albumin were normal in all but one patient with refractory protein losing enteropathy. Alanine aminotransferase, Aspartate aminotransferase and gamma glutamyltransferase levels were normal or only mildly elevated in the majority of patients. Alfa-1-antitrypsin excretion in the feces was normal (n=48) or only mildy elevated (n=3) in all patients.

8

Comprehensive MRI analysis

Multiparametric Liver imaging

Multiparametric liver imaging was performed in all patients. cT1 analysis could not be performed in one patient due to insufficient data quality. cT1 (reference 633-794ms) was elevated in all patients (mean cT1 964±63ms, range 824-1073ms). T2* was within normal ranges (reference value >12.5ms) in all patients (mean T2* 22.6±3.4ms). Mean PDFF (reference value <5.6%) was 1.7±3.3%. Only one patient had an elevated PDFF of 27.1% indicating liver steatosis.

Ventricular function and 4D flow MRI energetics

Mean cardiac index and ejection fraction were 3.4±0.09 L/min/m^2 and 48±7%, respectively. 4D flow MRI of the TCPC was acquired in 61 patients. One patient wanted to stop with the MRI examination before acquisition of 4D flow MRI was completed. Five patients were excluded from 4D flow analysis due to insufficient image quality (excessive patient movement related, n=4) or because of the presence of multiple central device-related artefacts affecting the majority of the TCPC. The total TCPC without device-related MR artefacts was available for 4D flow energetic analysis in 28/56 patients (50%).

In the patients in whom the entire TCPC was available for analysis, KE_{norm_flow} and EL_{norm_flow} in the total TCPC were 0.26±0.068 mJ per L/min and 0.075±0.022 mW per L/min inflow. Energetics were not significantly different between genders (p=0.27-0.37). A significant positive correlation was observed for KE_{norm_flow} and EL_{norm_flow} with cT1 (r=0.50, p=0.006 and r=0.39, p=0.04, respectively, Figure 1). An example of TCPC blood flow patterns, related energetics and cT1 liver mapping is shown for two extracardiac Fontan patients in Figure 2. Furthermore, KE_{norm_flow} and EL_{norm_flow} showed a significant negative correlation with peak VO2 (r=-0.61, p=0.003 and r=-0.54, p=0.009, respectively) and predicted % peak VO2 (r=-0.44, p=0.04 and r=-0.46, p=0.03, respectively, Figure 1). No significant correlations were found between cardiac index or ejection fraction with cT1 or (predicted) peak VO2.

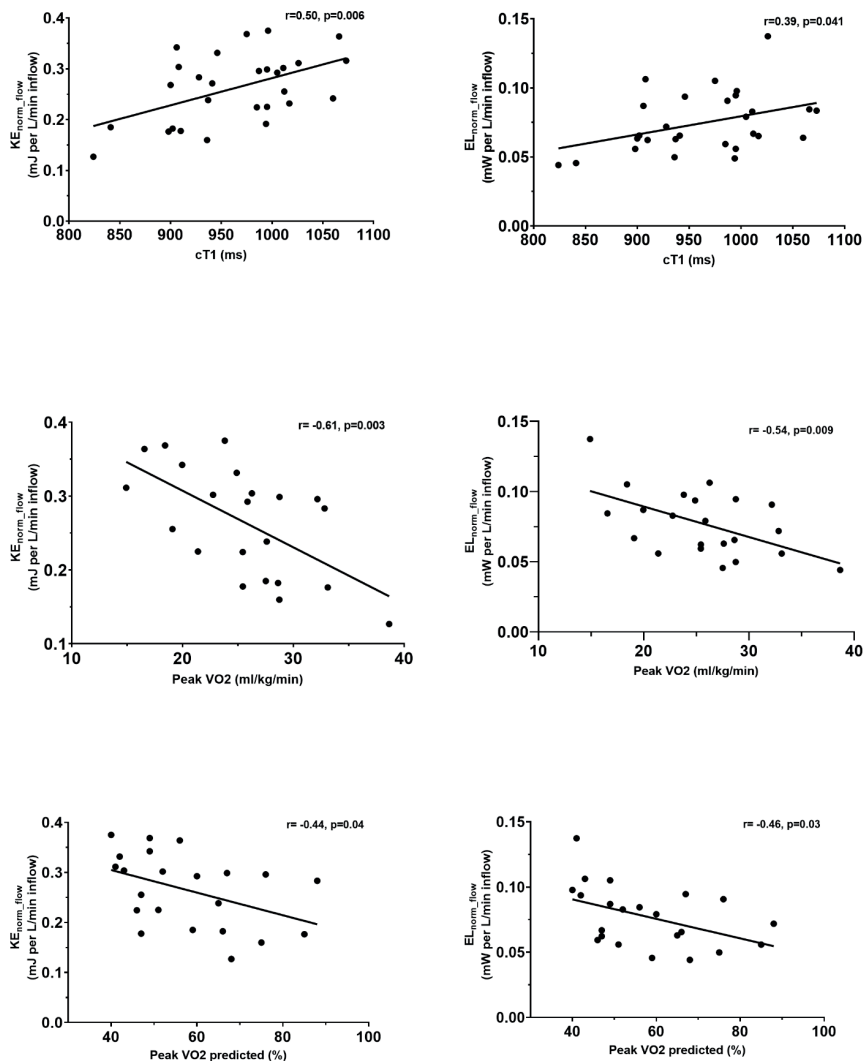**Figure 1.** Correlation analysis between KE (left) and EL (right) in the total TCPC with cT1 (upper panel), peak VO2 (middle panel) and predicted peak VO2 (lower panel) are shown.

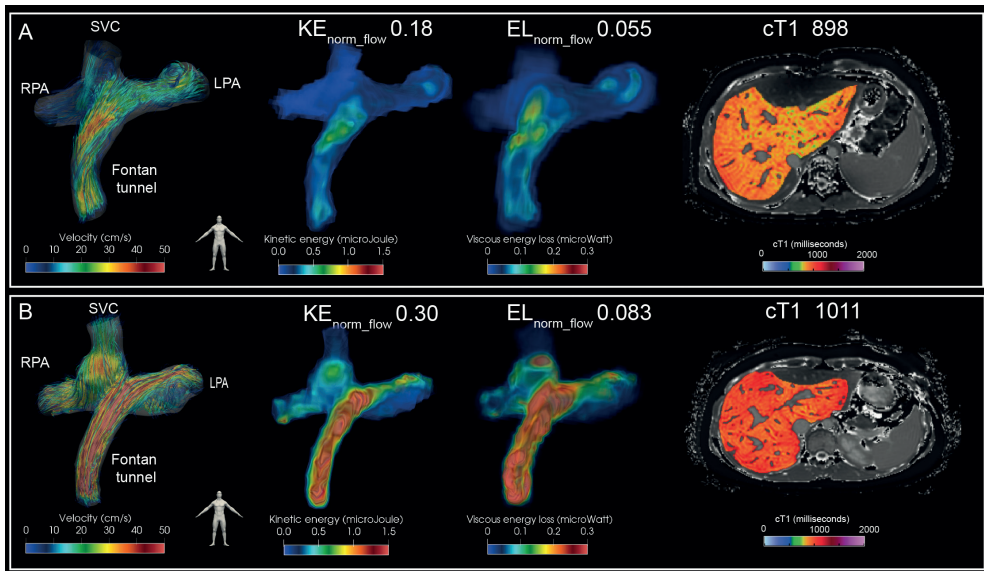*KE; kinetic energy, EL; viscous energy loss rate*

Figure 2. Streamline representation of blood flow in the TCPC is shown for two representative female extracardiac Fontan patients with a 16mm Goretex conduit (left panel) for the first phase of the cardiac cycle. Corresponding spatial distribution of KE and EL is shown (middle panels). The time-averaged normalized energetics values are indicated above. Whole liver cT1 mapping is shown for a transversal slice (right panel). Note how a strong difference in blood flow velocity is present at the level of the extracardiac conduit which is strongly correlated to the areas of increased KE and EL. Patient A: 17 years old, double inlet left ventricle + transposition of the great arteries, BSA 1.5. Patient B: 18 years old, tricuspid atresia, BSA 1.8.

BSA; body surface area, KE; kinetic energy, EL; viscous energy loss rate, cT1; iron-corrected T1 mapping, RPA/LPA; right/left pulmonary artery, SVC; superior vena cava.

Segmental 4D flow MRI energetics

Results of segmental TCPC energetics are reported in Table 4. $KE_{norm\_flow+length}$ was lowest in the SVC and lower compared to the Fontan tunnel ($p<0.001$), RPA ($p=0.002$) and LPA ($p<0.001$). $KE_{norm\_flow+length}$ was higher in the LPA compared to the RPA ($p=0.027$). $EL_{norm\_flow+length}$ was higher in the conduit ($p=0.024$) and LPA ($p<0.001$) compared to the SVC and higher in the LPA compared to the RPA ($p<0.001$). In the Fontan tunnel, mean CSA showed a strong negative correlation with $KE_{norm\_flow+length}$ ($\rho= -0.80$, $p<0.001$) and $EL_{norm\_flow+length}$ ($\rho= -0.78$, $p<0.001$, Supplemental Table 2). A weak correlation was found between mean LPA CSA and $EL_{norm\_flow+length}$ ($\rho= -0.31$, $p=0.034$). Energetics in the RPA and SVC were not related to segment-specific CSA.

Table 2. CPET results

$SBP_{basal,}$ mmHg	124(15)
$SBP_{peak,}$ mmHg	172(26)
RER_{peak}	1.1(0.09)
Power, watt	131(37)
% predicted	68(15)
HRrest, bpm	82(15)
HRpeak, bpm	172(17)
% predicted	93(10)
HRreserve, bpm	91(25)
Maximal exercise (n=50)	
VO2 peak, ml/kg/min	27.1(6.2)
% predicted	57(12)

Values are reported as mean (standard deviation). HRpeak: maximal heart rate at peak exercise; HRreserve: maximal heart rate-resting heart rate; HRrest: resting heart rate; RERpeak: respiratory exchange ratio at peak exercise; SBPbasal/peak: systolic blood pressure at rest/peak; VO2peak: oxygen uptake at peak exercise

Table 3. Laboratory results

	n	Mean (SD)	Range	Abnormal level, n (%)
Total protein, g/L	56	71(7)	35-83	1 (2)
Albumin, g/L	59	48(5)	18-54	1 (2)
Aspartate aminotransferase, U/L	57	32(10)	18-74	22 (39)
Alanine aminotransferase, U/L	58	36(16)	15-111	14 (24)
Gamma glutamyltransferase, U/L	56	58(40)	18-185	25 (45)
Total bilirubin, μmol/L	55	15(10)	5-49	13 (24)
INR*, (reference ≤1.2)	42	1.1(0.1)	1.0-1.5	3 (7)
Fecal alfa-1-antitrypsine, mg/g (reference <0.4)	51	0.2(0.1)	0.1-0.7	3 (6)

*Patients on oral anticoagulation were excluded. SD, standard deviation

Table 4. 4D flow MRI derived energetics in the TCPC

4D flow MRI	n	KE_{norm_flow}	EL_{norm_flow}
Total TCPC	28	0.260(0.068)	0.075(0.022)
Segmental analysis		$KE_{norm\_flow+length}$	$EL_{norm\_flow+length}$
Fontan tunnel	35	0.034(0.011)	0.0087(0.0029)
SVC	31	0.023(0.007)	0.0065(0.0024)
LPA	46	0.040(0.018)	0.012(0.005)
RPA	49	0.031(0.01)	0.0081(0.0032)
Fontan confluence	56	0.094*(0.041)	0.031*(0.013)

* Values are reported as mean (standard deviation). KE_{norm_flow} and EL_{norm_flow}. KE_{norm_flow} in mJ per L/min and EL_{norm_flow} in mW per L/min. $KE_{norm\_flow+length}$ in mJ per L/min per cm segment, $EL_{norm\_flow+length}$ in mW per L/min per cm segment. LPA/RPA; left/right pulmonary artery, SVC; superior vena cava, TCPC; total cavopulmonary connection, KE; kinetic energy, EL; viscous energy loss rate

8

Discussion

This study for the first time shows the relationship between in vivo 4D flow MRI-derived TCPC blood flow energetics, exercise capacity and MR-based assessment of liver fibrosis/congestion (cT1 mapping). Liver cT1 values were elevated in all patients at a mean age of 17 years, indicating universal liver fibrosis/congestion. KE_{norm_flow} and EL_{norm_flow} in the TCPC correlated with maximal exercise capacity and liver cT1, while conventional parameters as ventricular ejection fraction and cardiac index did not. The Fontan tunnel and LPA were the segments with most adverse energetics. EL_{norm_flow} was highest in patients with smallest Fontan tunnels raising concern on the current approach of Fontan completion with 16 to 20mm rigid conduits.

Surgical construction of an energy efficient TCPC with low resistance is important to keep the increase in CVP and reduction of preload towards the single ventricle to a minimum.[21] An elevated CVP and reduced cardiac output play an important role in the occurrence of liver fibrosis and decreased exercise capacity, respectively. In silico CFD modelling studies have identified PA stenosis and undersized Fontan tunnels to be associated with reduced flow efficiency[4, 5, 22], which correlates with liver fibrosis stage and exercise capacity.[6, 7] Therefore, routine screening of Fontan patients on the occurrence of (subclinical) adverse TCPC flow efficiency is clinically relevant for timely identification of patients with adverse TCPC hemodynamics, in whom intervention may be beneficial.

Recently, 4D flow MRI has emerged as a promising non-invasive technique for quantification of in vivo TCPC flow efficiency. KE and EL in the TCPC are novel 4D flow MRI markers reflecting TCPC flow efficiency, influenced by adverse TCPC geometry (e.g. PA stenosis or undersized conduit) and related flow patterns. 4D flow MRI previously revealed adverse vortical/helical flow patterns in the Fontan confluence, PAs, or in a blind-ending pulmonary trunk, all areas associated with increased KE and EL.[9, 19] In this study, adverse 4D flow derived KE and EL in the TCPC correlated with reduced maximal exercise capacity and increased levels of liver fibrosis/congestion (cT1), and may therefore be important novel markers that can indicate adverse outcome.

Exercise capacity

Decreased exercise capacity in Fontan patients is predominantly caused by a limited capability to maintain preload and stroke volume of the single ventricle during exercise.[2] Importantly, resting cardiac index and ejection fraction did not correlate with exercise capacity, but adverse 4D flow energetics in the TCPC did show a significant correlation. This might be explained by the fact that increased EL in the TCPC may particularly affect preload and thus cardiac output during exercise conditions only, since energy loss

in the TCPC increases non-linearly with exercise[23], and are therefore not captured by evaluation of resting cardiac function parameters.

Liver fibrosis

Presence of Fontan associated liver disease, including liver fibrosis, is universal in Fontan patients and the chronic exposure of the liver to an elevated CVP plays an important role.[1] The association between energetics and liver cT1 mapping can therefore be explained by the fact that elevated EL in the TCPC will require an increased CVP to maintain cardiac output. Fibrosis progression rate varies between patients and factors that lead to accelerated liver fibrosis are unknown as serial liver fibrosis assessment is lacking.[24] Future longitudinal studies with liver cT1 mapping could verify if patients with adverse TCPC energetics show faster progression in liver fibrosis.

Liver cT1 mapping

Gold standard liver biopsy is subject to sampling errors and its invasiveness prohibits routine serial assessment. In this study a novel non-invasive approach was used based on iron-corrected T1 mapping to quantify increased levels of extracellular liver fluid, which is elevated in liver fibrosis and/or venous congestion. Although cT1 values showed good correlation with histologic liver fibrosis in adult patients with liver disease[15], validation in Fontan patients is currently lacking. Especially venous congestion will influence T1 values in Fontan patients since increased CVP has been correlated with increased levels of liver T1.[25] Therefore, distinction between liver fibrosis or congestion due to increased CVP on elevated cT1 cannot be determined. However, since an increased CVP is associated with important morbidity such as PLE and liver fibrosis, measurement of cT1 as a combined marker of fibrosis/CVP is a promising non-invasive marker for adverse outcome.

8

Segmental analysis

Analysis of the TCPC segments that most severely affected the adverse energetics of the entire TCPC indicated that the Fontan tunnel and LPA are the areas to focus on for improved TCPC efficiency. Increased KE and EL in the conduit, carrying 70% of total systemic venous return, can be explained by the presence of undersized extracardiac conduits (IVC-conduit velocity mismatch) caused by somatic overgrowth[8], since a strong inverse correlation between conduit CSA and energetics was shown. LPA hypoplasia/ stenosis, often observed in hypoplastic left heart syndrome patients, but also the presence of vortical flow in larger LPAs or in patients in whom the pulmonary trunk has not been detached, can explain the adverse energetics in the LPA.[9, 19].

Limitations

Compared to CFD, 4D flow MRI underestimates "true" energy loss and only captures relatively large-scale flow structures due to a limited spatial resolution. However, the relative performance of the TCPC between patients remains intact making comparison of TCPC energetics between Fontan patients still possible.[26] 4D flow MRI also does not capture the influence of respiration on TCPC blood flow[27], which could significantly affect energy losses.[28] Novel 5D flow MRI sequences can be of interest to study the effect of respiration on TCPC energetics.[29] TCPC energetics could only be linked to current cT1 values in this study. Since the occurrence of liver fibrosis is presumably time-related, correlation of TCPC energetics with longitudinal cT1 mapping will be of interest and is subject to future research. Liver cT1 mapping has been shown to predict mortality and liver-related events in patients with chronic liver disease[30], but its prognostic value in Fontan patients is currently unknown. Finally, the Fontan confluence segment could not be directly compared with the other four segments since Fontan confluence energetics were normalized for inflow only.

Conclusion

Adverse 4D flow MRI derived kinetic energy and viscous energy loss rate in the TCPC significantly correlate with reduced exercise capacity and increased levels of liver fibrosis/congestion (cT1), while ventricular ejection fraction and cardiac index did not. Liver cT1 values were elevated in all patients indicating universal presence of liver fibrosis/congestion. The Fontan tunnel and LPA were the segments with most adverse energetics indicating potential room for improvement. 4D flow MRI is therefore promising as a non-invasive screening tool for identification of patients with adverse TCPC flow efficiency that may guide treatment strategies during follow-up.

References

1. Goldberg DJ, Surrey LF, Glatz AC, Dodds K, O'Byrne ML, Lin HC, Fogel M, Rome JJ, Rand EB, Russo P and Rychik J. Hepatic Fibrosis Is Universal Following Fontan Operation, and Severity is Associated With Time From Surgery: A Liver Biopsy and Hemodynamic Study. *J Am Heart Assoc*. 2017;6.

2. Paridon SM, Mitchell PD, Colan SD, Williams RV, Blaufox A, Li JS, Margossian R, Mital S, Russell J, Rhodes J and Pediatric Heart Network I. A cross-sectional study of exercise performance during the first 2 decades of life after the Fontan operation. *J Am Coll Cardiol*. 2008;52:99-107.

3. Haggerty CM, Restrepo M, Tang E, de Zelicourt DA, Sundareswaran KS, Mirabella L, Bethel J, Whitehead KK, Fogel MA and Yoganathan AP. Fontan hemodynamics from 100 patient-specific cardiac magnetic resonance studies: a computational fluid dynamics analysis. *J Thorac Cardiovasc Surg*. 2014;148:1481-9.

4. Rijnberg FM, Hazekamp MG, Wentzel JJ, de Koning PJH, Westenberg JJM, Jongbloed MRM, Blom NA and Roest AAW. Energetics of Blood Flow in Cardiovascular Disease: Concept and Clinical Implications of Adverse Energetics in Patients With a Fontan Circulation. *Circulation*. 2018;137:2393-2407.

5. Tang E, Restrepo M, Haggerty CM, Mirabella L, Bethel J, Whitehead KK, Fogel MA and Yoganathan AP. Geometric characterization of patient-specific total cavopulmonary connections and its relationship to hemodynamics. *JACC Cardiovasc Imaging*. 2014;7:215-24.

6. Trusty PM, Wei ZA, Rychik J, Graham A, Russo PA, Surrey LF, Goldberg DJ, Yoganathan AP and Fogel MA. Cardiac Magnetic Resonance-Derived Metrics Are Predictive of Liver Fibrosis in Fontan Patients. *Ann Thorac Surg*. 2020;109:1904-1911.

7. Khiabani RH, Whitehead KK, Han D, Restrepo M, Tang E, Bethel J, Paridon SM, Fogel MA and Yoganathan AP. Exercise capacity in single-ventricle patients after Fontan correlates with haemodynamic energy loss in TCPC. *Heart*. 2015;101:139-43.

8. Rijnberg FM, Elbaz MSM, Westenberg JJM, Kamphuis VP, Helbing WA, Kroft LJ, Blom NA, Hazekamp MG and Roest AAW. Four-dimensional flow magnetic resonance imaging-derived blood flow energetics of the inferior vena cava-to-extracardiac conduit junction in Fontan patients. *Eur J Cardiothorac Surg*. 2019;55:1202-1210.

9. Rijnberg FM, van Assen HC, Hazekamp MG and Roest AAW. Tornado-like flow in the Fontan circulation: insights from quantification and visualization of viscous energy loss rate using 4D flow MRI. *Eur Heart J*. 2019;40:2170.

10. Rijnberg FM, van Assen HC, Hazekamp MG, Roest AAW and Westenberg JJM. Hemodynamic Consequences of an Undersized Extracardiac Conduit in an Adult Fontan Patient Revealed by 4-Dimensional Flow Magnetic Resonance Imaging. *Circ Cardiovasc Imaging*. 2021;14:e012612.

11. Godfrey S. *Exercise testing in children: applications in health and disease*: Saunders Limited.; 1974.

12. Ten Harkel AD, Takken T, Van Osch-Gevers M and Helbing WA. Normal values for cardiopulmonary exercise testing in children. *Eur J Cardiovasc Prev Rehabil*. 2011;18:48-54.

13. Schaapman JJ, Tushuizen ME, Coenraad MJ and Lamb HJ. Multiparametric MRI in Patients With Nonalcoholic Fatty Liver Disease. *J Magn Reson Imaging*. 2021;53:1623-1631.

14. Kendall TJ, Stedman B, Hacking N, Haw M, Vettukattill JJ, Salmon AP, Cope R, Sheron N, Millward-Sadler H, Veldtman GR and Iredale JP. Hepatic fibrosis and cirrhosis in the Fontan circulation: a detailed morphological study. *J Clin Pathol*. 2008;61:504-8.

8

15. Banerjee R, Pavlides M, Tunnicliffe EM, Piechnik SK, Sarania N, Philips R, Collier JD, Booth JC, Schneider JE, Wang LM, Delaney DW, Fleming KA, Robson MD, Barnes E and Neubauer S. Multiparametric magnetic resonance for the non-invasive diagnosis of liver disease. *J Hepatol*. 2014;60:69-77.

16. Szczepaniak LS, Nurenberg P, Leonard D, Browning JD, Reingold JS, Grundy S, Hobbs HH and Dobbins RL. Magnetic resonance spectroscopy to measure hepatic triglyceride content: prevalence of hepatic steatosis in the general population. *Am J Physiol Endocrinol Metab*. 2005;288:E462-8.

17. Mojtahed A, Kelly CJ, Herlihy AH, Kin S, Wilman HR, McKay A, Kelly M, Milanesi M, Neubauer S, Thomas EL, Bell JD, Banerjee R and Harisinghani M. Reference range of liver corrected T1 values in a population at low risk for fatty liver disease-a UK Biobank sub-study, with an appendix of interesting cases. *Abdom Radiol (NY)*. 2019;44:72-84.

18. Elbaz MS, van der Geest RJ, Calkoen EE, de Roos A, Lelieveldt BP, Roest AA and Westenberg JJ. Assessment of viscous energy loss and the association with three-dimensional vortex ring formation in left ventricular inflow: In vivo evaluation using four-dimensional flow MRI. *Magn Reson Med*. 2017;77:794-805.

19. Rijnberg FM, Juffermans JF, Hazekamp MG, Helbing WA, Lamb HJ, Roest AAW, Westenberg JJM, van Assen HC and Nagy E. Segmental assessment of blood flow efficiency in the total cavopulmonary connection using four-dimensional flow magnetic resonance imaging: vortical flow is associated with increased viscous energy loss rate. *European Heart Journal Open*. 2021;1.

20. Juffermans JF, Westenberg JJM, van den Boogaard PJ, Roest AAW, van Assen HC, van der Palen RLF and Lamb HJ. Reproducibility of Aorta Segmentation on 4D Flow MRI in Healthy Volunteers. *J Magn Reson Imaging*. 2021;53:1268-1279.

21. Sundareswaran KS, Pekkan K, Dasi LP, Whitehead K, Sharma S, Kanter KR, Fogel MA and Yoganathan AP. The total cavopulmonary connection resistance: a significant impact on single ventricle hemodynamics at rest and exercise. *Am J Physiol Heart Circ Physiol*. 2008;295:H2427-35.

22. Dasi LP, Krishnankuttyrema R, Kitajima HD, Pekkan K, Sundareswaran KS, Fogel M, Sharma S, Whitehead K, Kanter K and Yoganathan AP. Fontan hemodynamics: importance of pulmonary artery diameter. *J Thorac Cardiovasc Surg*. 2009;137:560-4.

23. Whitehead KK, Pekkan K, Kitajima HD, Paridon SM, Yoganathan AP and Fogel MA. Nonlinear power loss during exercise in single-ventricle patients after the Fontan: insights from computational fluid dynamics. *Circulation*. 2007;116:I165-71.

24. Evans WN, Acherman RJ, Mayman GA, Galindo A, Rothman A, Winn BJ, Yumiaco NS and Restrepo H. The Rate of Hepatic Fibrosis Progression in Patients Post-Fontan. *Pediatr Cardiol*. 2020;41:905-909.

25. de Lange C, Thrane KJ, Thomassen KS, Geier O, Nguyen B, Tomterstad A, Ording Müller LS, Thaulow E, Almaas R, Døhlen G, Suther KR and Möller T. Hepatic magnetic resonance T1-mapping and extracellular volume fraction compared to shear-wave elastography in pediatric Fontan-associated liver disease. *Pediatr Radiol*. 2021;51:66-76.

26. Cibis M, Jarvis K, Markl M, Rose M, Rigsby C, Barker AJ and Wentzel JJ. The effect of resolution on viscous dissipation measured with 4D flow MRI in patients with Fontan circulation: Evaluation using computational fluid dynamics. *J Biomech*. 2015;48:2984-9.

27. van der Woude SFS, Rijnberg FM, Hazekamp MG, Jongbloed MRM, Kenjeres S, Lamb HJ, Westenberg JJM, Roest AAW and Wentzel JJ. The Influence of Respiration on Blood Flow

in the Fontan Circulation: Insights for Imaging-Based Clinical Evaluation of the Total Cavopulmonary Connection. *Front Cardiovasc Med*. 2021;8:683849.

28. Tang E, Wei ZA, Trusty PM, Whitehead KK, Mirabella L, Veneziani A, Fogel MA and Yoganathan AP. The effect of respiration-driven flow waveforms on hemodynamic metrics used in Fontan surgical planning. *J Biomech*. 2019;82:87-95.

29. Bastkowski R, Bindermann R, Brockmeier K, Weiss K, Maintz D and Giese D. Respiration Dependency of Caval Blood Flow in Patients with Fontan Circulation: Quantification Using 5D Flow MRI. *Radiol Cardiothorac Imaging*. 2019;1:e190005.

30. Pavlides M, Banerjee R, Sellwood J, Kelly CJ, Robson MD, Booth JC, Collier J, Neubauer S and Barnes E. Multiparametric magnetic resonance imaging predicts clinical outcomes in patients with chronic liver disease. *J Hepatol*. 2016;64:308-315.

8

Supplementary materials

Supplemental Table 1. 4D flow MRI acquisition details

No. of slices (orientation)	27 (coronal)
Field of view, mm	350x271x56
ECG-gating	Retrospective
No. of reconstructed cardiac phases	24
No. of signal averages	1
Respiratory compensation	navigator
Typical navigator efficiency	40-60%
Acquired spatial resolution (mm)	2.4x2.4x2.4
Reconstructed spatial resolution (mm)	2.1x2.1x2.1
Acquired temporal resolution, ms (SD)	32.0
Flip angle (°)	10
TE (ms)	4.5
TR (ms)	8.0
VENC (cm/s)	80
Typical scan time (minutes)	12-18
Acceleration methods	SENSE factor 1.5, RL direction, EPI factor 5, Segmentation factor 1

SD; standard deviation, ms; milliseconds, mm; millimeter, TE; echo time, TR; repetition time, VENC; velocity encoding, SENSE; sensitivity encoding, AP; anterior-posterior, EPI; echo planar imaging readout, ECG; electrocardiogram

Supplemental Table 2. Correlation analysis between cross-sectional area of the TCPC segments and 4D flow MRI energetics

	n	CSA (mm^2/m^2)	KE$_{norm\_flow+length}$		EL$_{norm\_flow+length}$	
			Correlation coefficient	p	Correlation coefficient	p
Fontan tunnel	35	106 (91-134)	-0.80	**<0.001**	-0.78	**<0.001**
SVC	31	96 (76-109)	0.23	0.21	-0.02	0.93
LPA	46	92 (70-113)	0.03	0.85	-0.31	**0.034**
RPA	49	88 (81-101)	-0.10	0.48	-0.10	0.50

Correlation coefficients represent Pearson or Spearman rank analysis. SVC; superior vena cava, LPA/RPA; left/right pulmonary artery, CSA; cross-sectional area normalized for body surface area, TCPC; total cavopulmonary connection, KE; kinetic energy, EL; viscous energy loss rate